Journal of Polymers and the Environment (2023) 31:1812–1827
https://doi.org/10.1007/s10924-022-02675-z

ORIGINAL PAPER

Alginate Biopolymer FeNi Nanocomposite Blend Stabilizes Cu Nanoparticles Template for Hydrogenation of Nitrophenol and dyes Discoloration

Youssef O. Al-Ghamdi[1]

Accepted: 4 November 2022 / Published online: 13 December 2022
© The Author(s), under exclusive licence to Springer Science+Business Media, LLC, part of Springer Nature 2022

Abstract
In the current work, alginate (Alg) biopolymer was blended with FeNi nanoparticles (Alg-FeNi) in 1, 3, and 5 weight% and are described as Alg-FeNi1, Alg-FeNi3, and Alg-FeNi5 respectively and are cross-linked by using $CaCl_2$ as a cross-linker. This different Alg-FeNi blend was a solid supporting medium for stabilizing Cu NPs (Cu@Alg-FeNi). The synthesized catalyst was characterized through FESEM, EDS, Raman, and XRD. The templates of Cu@Alg-FeNi1-5 were used as dip-catalysis for the hydrogenation of 4-nitrophenol (4NP) and discoloration of methylene blue (MB) and methyl orange (MO) dyes in an aqueous medium by using $NaBH_4$ as a reductant. Various kinetics models were used to deduce the rate constant (k_{app}) and R^2 values for the degradation reactions. By increasing the amount of FeNi, the reaction rate was also enhanced for all three model pollutants, and Cu@Alg-FeNi5 exhibited the most potent catalyst activity. The k_{app} and R^2 value derived from zeroth order kinetics was 3.8×10^{-1} min^{-1} and 0.9188 R^2 values. In the case of 4NP, MB, and MO dyes, the experimental data were well-fitted in zero-order kinetics, suggesting that the reaction rate is independent of the reactant concentration. Simultaneous removal of 4NP and MB indicated its practical applicability, and the catalyst showed good recyclability.

Keywords Alginate-FeNi beads · characterization · pollutant degradations

Introduction

Heterogenous and homogenous catalysis is essential catalyst systems for various industrial and technological applications [1]. In homogenous, the catalyst is in the same phase as the reaction medium; therefore, keeping it in the stabilized form is challenging. The process of aggregation and agglomeration is frequent in homogenous catalysis, which decreases their reactivity. Although surfactants are used for such catalyst systems, they are still not frequently used on a large scale. Contrary, heterogenous catalysis has a different phase than the reaction medium. A solid support is usually used to stabilize the nanoscale materials. The most active nanoscale material is zero-valent metal nanoparticles. Zero-valent metal nanoparticles use solid support for their stabilization. In the past few decades, various templates have been synthesized to stabilize zero-valent metal nanoparticles, for instance, TiO_2, ZnO, metal oxide support, plant materials, polymer, and polymer-based nanocomposites. Among the different supporting materials, polymer-based nanocomposite proved one of the most suitable supporting matrixes [2]. Various polymers have been used for this purpose, including chitosan, cellulose, cellulose acetate, polyvinyl alcohol, polyether sulphone, and many others; however, among them, alginate is one of the most important ones, owing to their biocompatibility, biodegradability, low cost, ease in availability and sustainable nature make it a good candidate in food, pharmaceutical, engineering, biomedical and environmental applications [3]. Alginate is the only polysaccharide with -COOH functional groups in each of the repeating units of the polymer [4]. Alginate polymer is blended with FeNi nanocomposite in the current study to make nanocomposite beads that interact with the polymer internetworking, increase their porosity and mechanical strength, and provide a solid supporting surface to the membrane for NPs stabilization. Composite materials are an emerging field in science and technology, where the matrix offers room for the inorganic filler or reinforced materials and fix them in

✉ Youssef O. Al-Ghamdi
yo.alghamdi@mu.edu.sa

[1] Department of Chemistry, College of Science Al-Zulfi, Majmaah University, Al-Majmaah 11952, Saudi Arabia

the polymer networking [4]. Such catalyst systems are used mainly against the reduction of nitroarenes and discoloration of dyes.

Various procedures have been reported to reduce nitroarenes and discoloration of dyes. For instance, adsorption, membrane technology, advanced oxidation process, and supported nano-catalysis are some techniques used for wastewater treatment. Supporting catalysts are the most promising techniques [5]. Synthetic polymers dominated various industrial sectors in the past few decades due to their large-scale applications. However, natural polysaccharide is adopting its place in large-scale applications. Many researchers are now focusing on the natural polysaccharide polymer development on making novel materials by increasing their membrane processing capacity in various industrial applications [6–16]. Adding nanoscale materials to the polymer host can increase various characteristics of the polymer [2]. Nanomaterial substances are classified as materials in which one dimension is less than 100 nm. Particles at the nanoscale can abruptly increase their chemical and physical characteristics [1]. Therefore, nanocomposite materials have much better characteristics than bared polymers [2].

4-nitrophenol reduction is one of the most reliable reactions to evaluate the catalyst activity of such catalyst systems [2, 17–22]. 4-nitrophenol is one of the most nitroarene aromatic compounds which finds many applications in various industries such as agriculture, dyes synthesis, pharmaceuticals, and others. Due to their side effects on living organisms, The U.S environmental protection agency announced the removal of nitrophenols on a priority basis from wastewater. 4-nitrophenols is primarily used for herbicide, fungicide, insecticides, synthetic dye synthesis, and various explosive [17, 23]. Owing to their vast applications in a variety of industrial manufacturing, it is dumped in the water bodies where it accumulates in the water bodies for a longer time and reaches our drinking water resources directly or indirectly, thus causing server damage to the living organism, if present more significant than the permissible limit. 4NP is an aromatic organic compound with excessive use in manufacturing industries such as pharmaceuticals, agriculture, fabrics, and dyes. Owing to their excessive use on a large scale, 4NP have multiple adverse effects on the kidney, CNS, lungs, and stomach. Therefore, its remediation is significant [1].

Dyes are another organic pollutant that is not used correctly. For instance, in ancient times, people made their environment gorgeous by using dyes and stuff; even our clothes, medicine, food, beverages, and much other daily life stuff are color in nature [24, 25]. However, the industrial setup directly dumped their extra/waste dyes and their things into the water resources, which is not esthetically good because dye traces block the passage of oxygen and solar light to the water. Therefore, dye and its derivatives directly or indirectly affect the living organism. Over the past few decades, interest has been developed in the manufacturing of synthetic dye, and on an approximation, over 7,000 tons of dye are manufactured annually. European Union made a policy to send zero synthetic chemicals to the water resources because some dyes and their degraded product are toxic and carcinogenic [25, 26]. MB is a cationic dye of the thiazine family with an immense blue coloration. The sharp color of the MB dye stops the diffusion and passage of sunlight and air in the water bodies if discharged. MO dye is an anionic mono-azo dye with deep orange color and has excessive use in academic and industrial sectors. The azo linkage was destroyed in reaction with $NaBH_4$ to make its hydrazine form. However, the hydrazine group cannot swiftly degrade with $NaBH_4$. Thus, the reaction is not kinetically economical [25].

Thus, in the current study, the Alg-FeNi1-5 blend was synthesized to stabilize Cu NPs and was used to reduce nitrophenols and discoloration of dyes.

Experimental

Reagent and Materials

Sodium Alginate (CAS NO. 9005-38-3), Sodium Borohydride powder (CAS NO. 16940-66-2), Methyl orange (CAS NO: 547-58-0) were purchased from DAEJUNG CHEMICALS, and METALS CO. LTD. Methylene blue (CAS NO. 61-73-4) and methyl orange were purchased from BDH CHEMICALS. Copper (II) sulfate pentahydrate (CAS NO. 7758-99-8), and 4-Nitrophenol (CAS NO. 100-02-7), were purchased from SIGMA-ALDRICH COMPANY.

Synthesis of FeNi Catalyst

for the synthesis of the FeNi catalyst, 0.1 M solutions of each $FeCl_3$ and $NiCl_2$ were mixed to make a 200 mL solution. After continuous stirring, the pH of the solution was adjusted with NaOH solution in a dropwise fashion and continuously monitored till the pH reached 9. Afterward, the reaction progressed at 70°C and continued stirring for six h. After completing the response, the precipitate was washed with the ethanol-water mixture 1:1 and centrifuged multiple times. After washing and centrifugation, the residue was dried in an oven at 80°C for six h and then calcined in a furnace at 400°C for five h. The FeNi catalyst was stored and used as an inorganic filler to the alginate biopolymer host for beads formation.

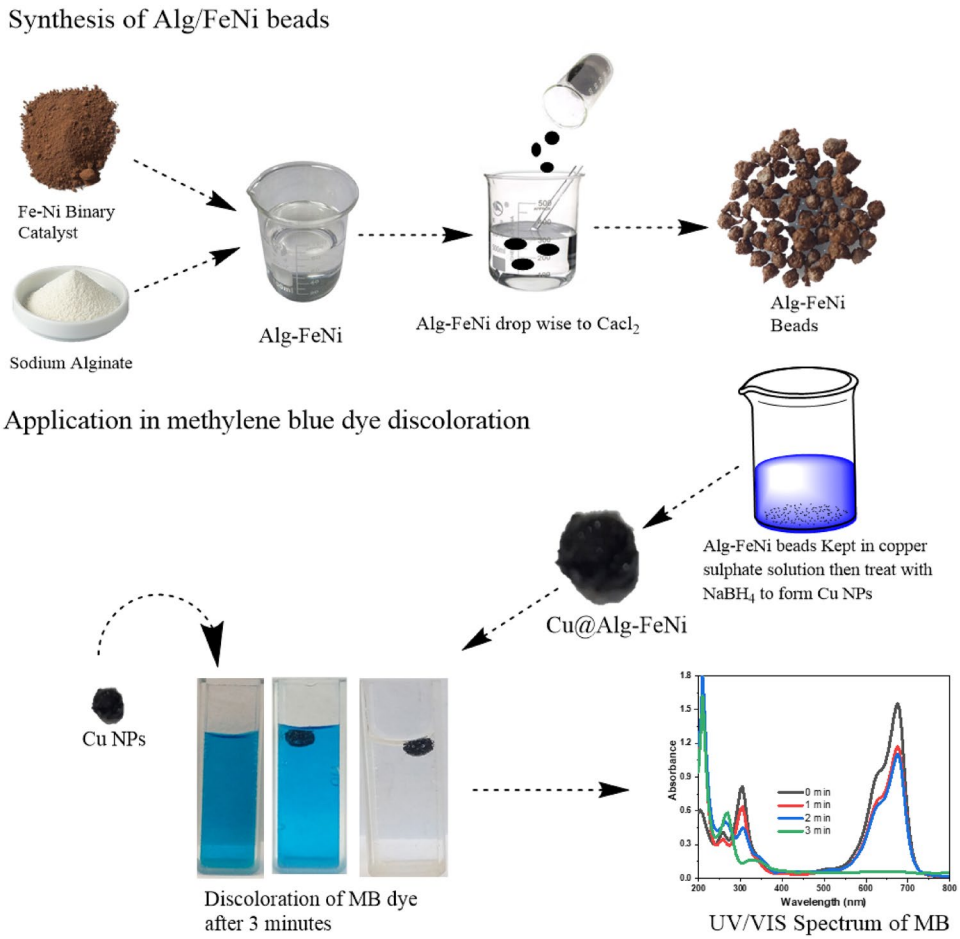

Scheme 1 Synthesis of Cu@Alg-FeNi NPs and its application in the discoloration of MB dye

Synthesis of Alg-FeNi Beads

For the synthesis of Alg-FeNi beads, firstly, 2 g alginate biopolymer was dissolved in 100 mL distilled water for 15 min at 100 °C. After the dope solution, the FeNi catalyst was added in different weight percentages, such as 1, 3, and 5%, to the 20 mL prepared alginate solution and stirred continuously through a stirrer to make a homogenous mixture of Alg-FeNi. After that, the Alg-FeNi mixture was dropped in an aqueous solution of 1 g/20mL $CaCl_2$ through a micro syringe to make the Alg-FeNi beads and remain in the solution for three hours. In the end, the beads were washed with distilled water, dried in an open atmosphere at room temperature, and stored for further use. The synthesized beads were termed Alg-FeNi1, Alg-FeNi3, and Alg-FeNi5 beads. It is worth mentioning here that pure alginate beads were synthesized similarly, as discussed above. However, the pure alginate beads were fragile and dissolved in the water, so we could not use them in further applications.

Synthesis of Alg-FeNi Beads Fabricated Cu NPs

Zero-valent Cu NPs fabricated with Alg-FeNi1-5 templates were synthesized by putting each bead separately in 30 mL of 10 mM copper sulfate pentahydrate solution for six h. the six ions were adsorbed on the active sites of each template and then treated with freshly prepared $NaBH_4$ solution to make Cu NPs. The Cu NPs supported on each bead were termed Cu@Alg-FeNi1, Cu@Alg-FeNi3, and Cu@Alg-FeNi5 catalysts, respectively. The synthetic procedure is enclosed in Scheme 1.

Evaluation of Catalyst in Degradation of Organic Pollutants

for the discoloration of MB and MO dye, 0.05 mM of both dyes were selected. From this stock solution, 2.5 mL was mixed with 0.5 mL of 10 mM $NaBH_4$ solution in a UV cuvette along with 30 mg of the catalyst. The MB or MO discoloration reaction was monitored at 664 and 464 nm,

respectively, in UV-Vis. absorbance spectrum. Similarly, the 4NP (2.5 mL of 0.1 mM) was mixed with 0.5 mL of 10 mM $NaBH_4$ solution along with 30 mg of the catalyst in a UV cuvette, and the absorbance decreased at 400 nm was monitored for 4-nitrophenolate anions.

For the concurrent degradation of 4NP (2.5 mL of 0.1 mM) and MB dye (2.5 mL of 0.05 mM), both the solutions were mixed in a vial, and then 0.5 mL of 10 mM $NaBH_4$ solution was added, due to which the color of the solution was yellow bluish. However, the maximum wavelength of 4-nitrophenolate and MB was changed from 400 to 415 nm and 664 to 675 nm, respectively, and the decrease in absorption of the mixture was monitored at 415 and 675 nm, respectively. The following Eqs. 1–4 was used to calculate the zeroth, pseudo 1st, 1st, and 2nd order kinetics, respectively. In contrast, Eq. 5 was used to deduce the percentage degradation of nitrophenol or dye or a mixture of nitrophenol and dye [20].

$$d[A] = -kdt + C \tag{1}$$

$$\ln[A]_t/A_0 = -kt + C \tag{2}$$

$$\ln[A] = -kt + C \tag{3}$$

$$1/[A]_t = -kt + 1/[A]_0 \tag{4}$$

$$\text{Percent degradation} = \left(\frac{A_0 - A_t}{A_t}\right) \times 100 \tag{5}$$

In Eq. 1, the variables are concentration vs. time and $\ln[A]_t/[A]_0$ vs. time is the variable in Eq. 2. Similarly, $\ln[A]$ vs. time is the variable in Eq. 3 while $1/[A]_t$ vs. time is the variable in time [27].

Recyclability of the Catalyst

The recyclability test was selectively performed with Cu@Alg-FeNi5 catalyst and 4NP as the model pollutant. The recyclability test was performed till the 5th cycle. After completing the first cycle, the catalyst was fed to 2nd and 3rd cycles, and so on. In each process of the recyclability test, 2.5 mL of 0.1 mM 4NP was put in the cuvette, and 0.5 mL of 10 mM $NaBH_4$ solution was added. To the cuvette, 40 mg of the catalyst was added, and the reaction progress was recorded in time-dependent UV-Vis. Spectrophotometer. The same catalyst was used in all five cycles for the 4NP solution in the presence of $NaBH_4$. It is worth mentioning that the catalyst is used without any treatment and directly used in the next cycle without washing or chemical or physical treatment.

Instrumentation

The weight of the reagents and catalyst was weighted through OHAUS analytical balance. Perkin Elmer Lambda 365 UV/Vis. The spectrophotometer was used to record the degradation of nitrophenol and dyes. Textural properties and elemental composition were recorded through FESSEM and EDX model JSM-IT-100 JEOL Japan and JDX-3532 JEOL XRD; Japan aided with Kα λ = 15 nm was employed to investigate the crystalline nature of the catalyst. Raman-532 Tec-Ci of Technospex Company Singapore was used for the Raman scattering experiment. For heating purposes, Dragon Lab MS7-H550-Pro Hot plate-aided magnetic stirrer was used.

Results and Discussion

Characterization

FESEM

The left side of Fig. 1a–c is the external surface, and the right side of FESEM images is the beads' internal surface. The left side of Fig. 1a indicates a rough surface area for Cu@Alg-FeNi1, where the small spherical Cu NPs are embedded in the polymer networking. In contrast, the right-side image showed an array of elongated polymer tubes enclosing small particles of Cu NPs. These long tubes are connected to make a continuous channel. Some flakes appeared among the various extended tubes suggesting the presence of FeNi NPs. Figure 1b left sides indicated a rough surface with embedded Cu NPs. The right side of Fig. 1b states a mixture of elongated tubes and smooth sheets. However, these sheets are made from merging tubes by zooming the image. Cu NPs are embedded inside the polymer network in both tubes and sheets. The Cu@Alg-FeNi3 shows a rough exterior surface with cracks and a few microvoids in which the Cu NPs protruded from the surface (Fig. 1c left side). The right side FESEM image of Cu@Alg-FeNi3 indicated nanotube polymer channels. By zooming the image, the Cu NPs are embedded in the tubes, while beneath these tubes, some amorphous stuff suggests the presence of FeNi NPs.

EDS

Figure 2a indicates the FESEM images from which the elemental window is extracted. The primary window shows peaks for C, O, Na Fe, Ni, and Cu by 15.05, 39.55, 3.33, 8.23, 2.36, and 31.48 elements by weight%, respectively, showing the purity of the catalyst. Figure 2b shows the FESEM images of Cu@Alg-FeNi3 as indicated on the left side from which peaks are various elements extracted,

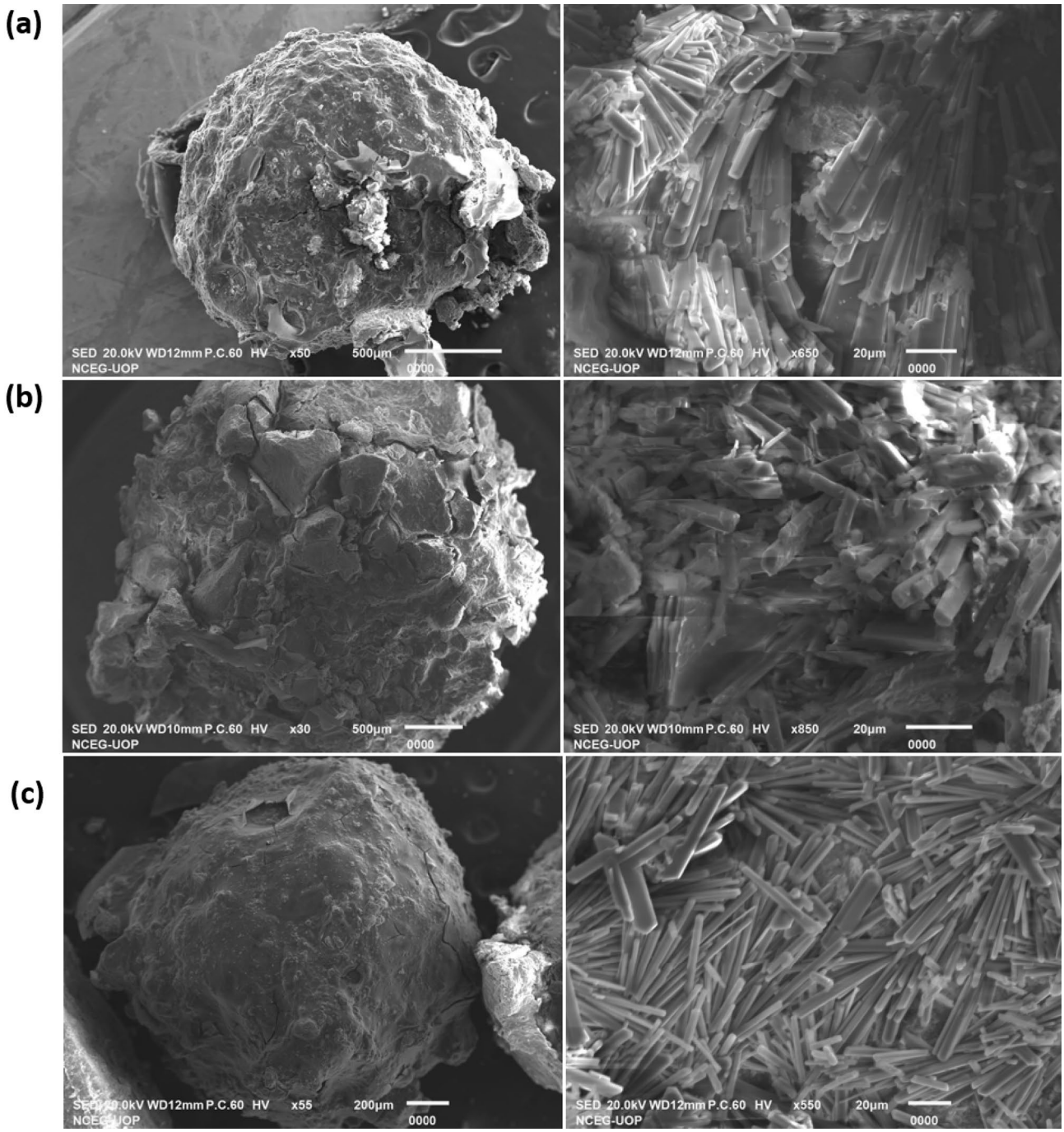

Fig. 1 FESEM images of Cu@Alg-FeNi1 (**a**), Cu@Alg-FeNi3 (**b**), and Cu@Alg-FeNi5 (**c**). The left pictures are the surface, and the right side is the internal view of the beads

for instance, C, O, Na, Fe, Ni, and Cu elements, which are present by 14.53, 46.53, 4.51, 9.84, 2.43, and 22.13 by weight% respectively. Thsignificfactorsements in the element window of Cu@Alg-FeNi3 are C, O, Na, Fe, Ni, and Cu elements. These elements are present in the catalyst backbone, indicating the purity of the catalyst. Similarly, the C, O, Na, Fe, Ni, and Cu elements appeared in 8.15, 37.28, 8.01, 17.83, 5.95, and 22.77 by weight%, respectively. The elemental window shows peaks for the above aspects in the Cu@Alg-FeNi5 catalyst, suggesting the purity of the sample as shown in the inset of Fig. 2c.

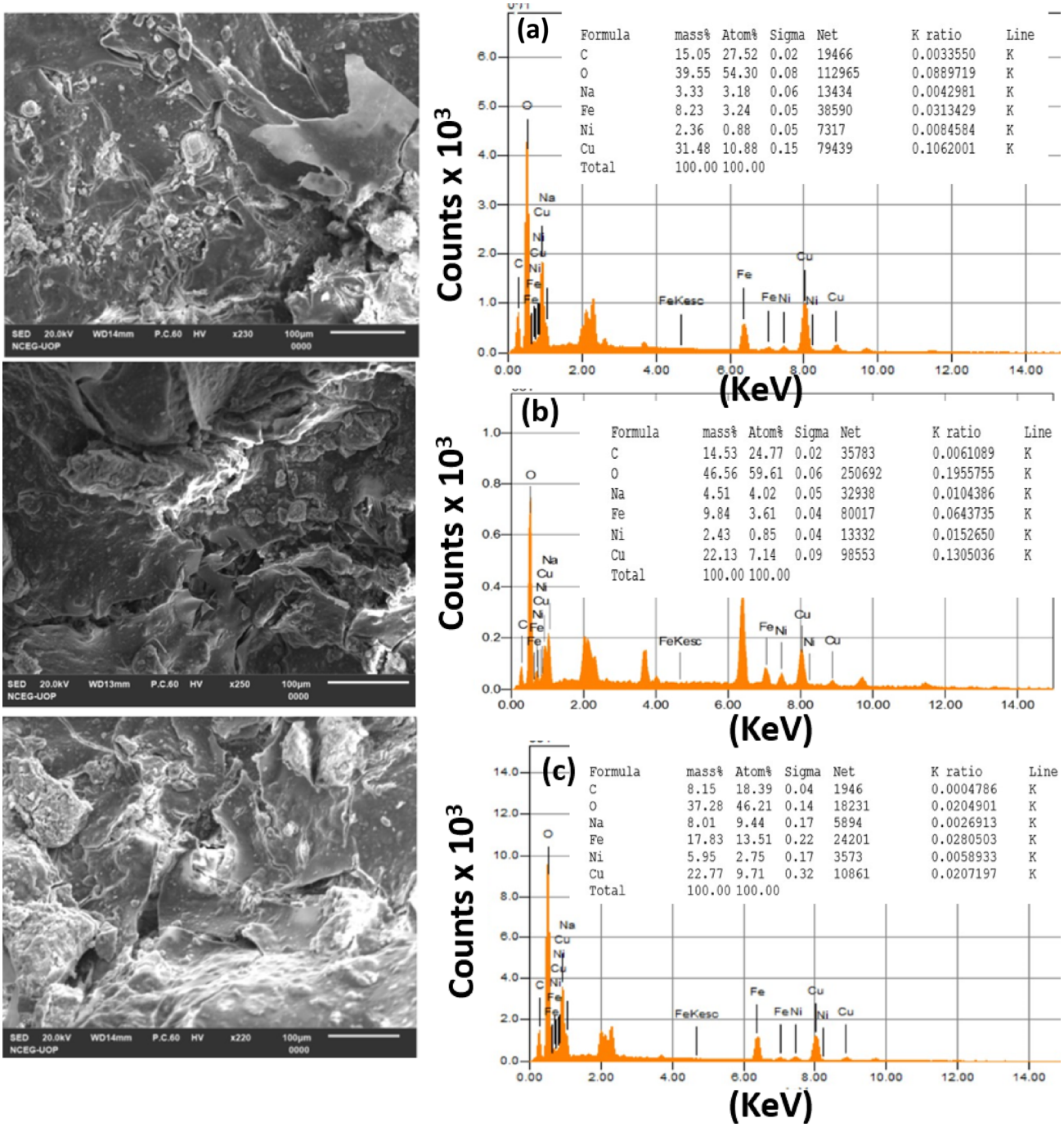

Fig. 2 Left side is the FESEM images from which the elemental window is extracted (right side) for: **a** Cu@Alg-FeNi1, **b** Cu@Alg-FeNi3, and **c** Cu@Alg-FeNi5.

Raman Spectroscopy

A Raman scattering experiment was performed to analyze the chemical structure of all three catalysts (Fig. 3a). The spectrum shows many noises; however, some identifiable peaks originated in all three catalysts. Peaks originating in the 550–610 cm^{-1} were due to the FeNi oxides or Cu NPs in all three catalysts [28]. The slight shifts in these values in all three catalysts were due to the different interactions. An embedded peak in the 1000 cm^{-1} is due to a glycosidic ring of the Na or Ca alginate ring. A peak at the range of 1250 cm^{-1} was represented by C–O bond stretching vibrations. The peaks at 1516 cm^{-1} were due to the carboxylate symmetric stretching vibration. This vibration is a little

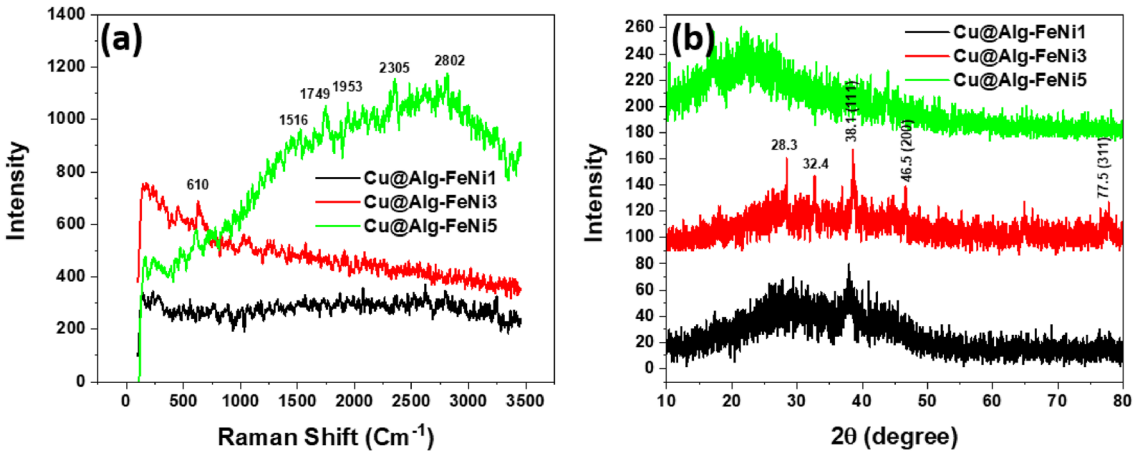

Fig. 3 Raman scattering (**a**) and XRD (**b**) of all three catalysts

lower than the reported data for Na or Ca alginate, which might be due to the linkage of FeNi or Cu NPs, which elongate the bond length, thus reducing the vibration energy of the bond length. The asymmetric C–H and O–H exhibited between 2800 and 3250 cm^{-1} [29].

XRD

The XRD indicated amorphous and crystalline peaks for all three catalysts, as shown in Fig. 3b. A broad hump at approximately 2θ = 23–26° in all three catalysts was due to the amorphous nature of the polymer. A small intense peak for the crystalline Cu NPs appeared at 77.5, corresponding to the (311) planes in the Cu@Alg-FeNi1 catalyst. Similarly, a peak at 2θ = 38.1° (111) was exhibited in Cu@Alg-FeNi3 and Cu-Alg-FeNi5 catalysts, suggesting zero-valent Cu NPs. However, some other peaks for copper oxide appeared in the Cu@Alg-FeNi3 catalyst. The XRD data indicated that well-crystalline zero-valent Cu NPs are anchored on the Alg-FeNi template.

Catalyst Evaluation

The catalyst activity was observed against the 4NP, MB, and MO dyes. The concurrent degradation of 4NP and MB dyes, while the catalyst recyclability was carried out against the reduction of 4NP by using Cu@Alg-FeNi5 catalyst in the presence of $NaBH_4$ as a reductant. All the catalyst activities are described one by one in the following section.

Reduction of 4NP

The 4NP is a ubiquitous organic compound that can be used to monitor the catalyst activity of a catalyst in UV-Vis. Spectrophotometer, because the product is only 4-aminophenol (4-AmP). This is a green reaction with no side effects. The reductant used to reduce 4NP is $NaBH_4$, but another reductant can also be used.

As evident from Fig. 4a, the reduction of 4NP to AmP was carried out with $NaBH_4$ only without a catalyst, where no significant change occurred. This is due to the stable bond of $–NO_2$ and the high activation energy needed to convert 4NP to 4AmP. However, after adding Cu NPs supported on different stabilizing matrixes such as Alg-FeNi1, Alg-FeNi3, and Alg-FeNi5 (Fig. 4b–d), the rate of reaction is swift. The highest activity was achieved with Cu@Alg-FeNi5 NPs in the presence of $NaBH_4$. Thus, it is inferred from the graph that Cu NPs cum $NaBH_4$ is responsible for the reduction of 4NP to AmP, which reduces the activation barrier of the reaction. In the current work, the stabilizing template

Table 1 Rate constant and R^2 values derived from various kinetics models

Entry	Zero-order		Psuedo-1st		1st order		2nd order		Degradation	Time
	k_{app}	R^2	k_{app}	R^2	k_{app}	R^2	k_{app}	R^2	%	min^{-1}
$NaBH_4$	4.6×10^{-3}	0.8619	4.0×10^{-3}	0.8629	4.0×10^{-3}	0.8629	3.5×10^{-3}	0.8640	3.0	10
Cu@Alg-FeNi1	2.1×10^{-2}	0.9269	4.5×10^{-1}	0.8388	4.5×10^{-1}	0.8388	0.2×10	0.6528	93.0	5
Cu@Alg-FeNi3	2.8×10^{-1}	0.9444	6.1×10^{-1}	0.8016	6.1×10^{-1}	0.8016	0.2×10	0.5959	92.0	4
Cu@Alg-FeNi5	3.8×10^{-1}	0.9188	8.8×10^{-1}	0.8332	8.8×10^{-1}	0.8332	0.4×10	0.6820	93.0	3

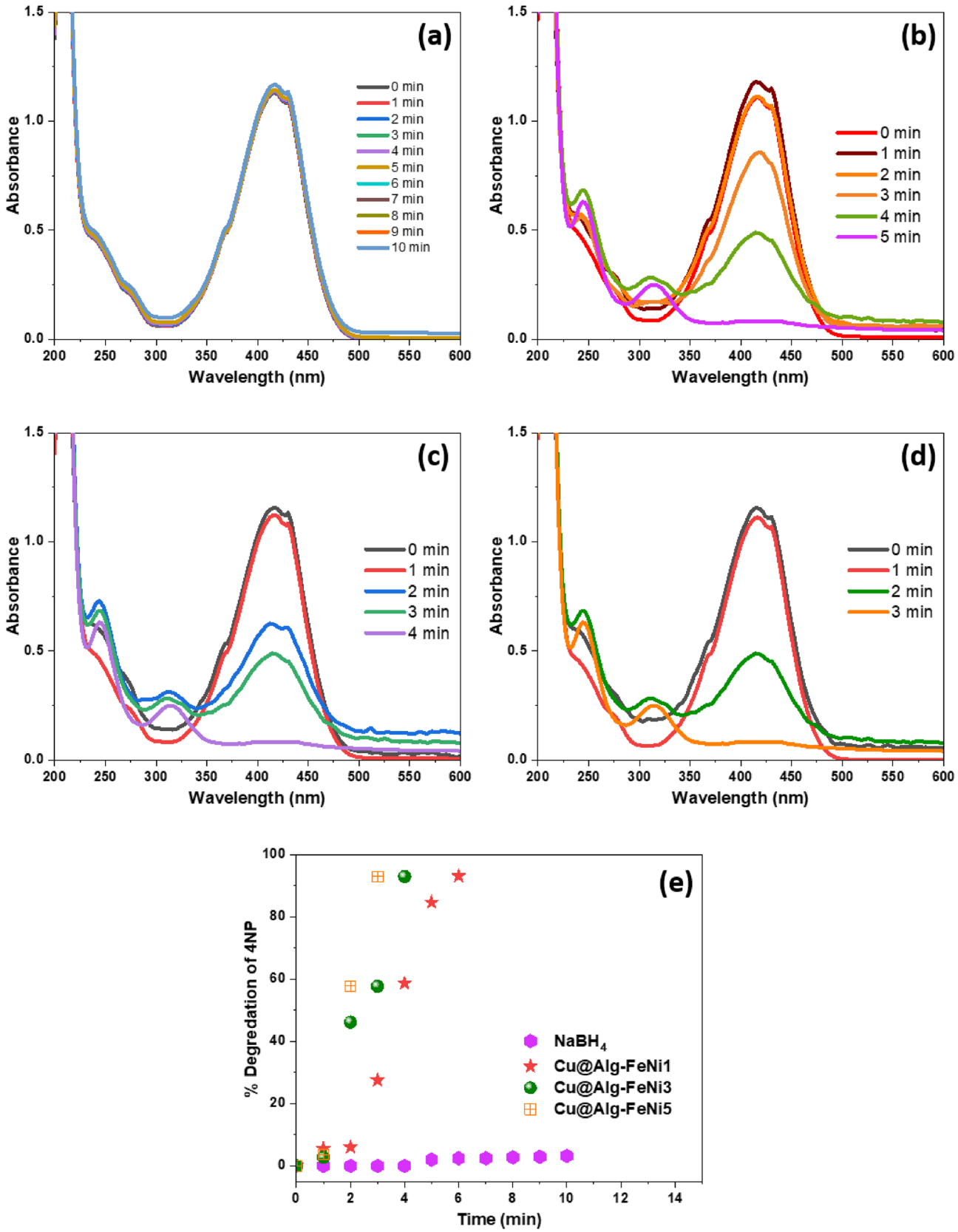

Fig. 4 UV-Visible spectrum of 4NP reduction with $NaBH_4$ (**a),** Cu@Alg-FeNi1 (**b),** Cu@Alg-FeNi3 (**c**), Cu@Alg-FeNi5 (**d**), % degradation of 4NP (**e**)

Table 2 Rate constant and R^2 values of MB dyes derived from various kinetics models

Entry	Zero-order		Psuedo-1st		1st order		2nd order		Degradation	Time
	k_{app}	R^2	k_{app}	R^2	k_{app}	R^2	k_{app}	R^2	%	min^{-1}
$NaBH_4$	3.1×10^{-2}	0.5919	2.4×10^{-3}	0.6106	2.4×10^{-3}	0.6106	1.8×10^{-3}	0.6486	29	9
Cu@Alg-FeNi1	2.9×10^{-2}	0.9091	5.4×10^{-1}	0.6472	5.4×10^{-1}	0.6472	0.24×10	0.4697	96	5
Cu@Alg-FeNi3	4.7×10^{-1}	0.9165	8.2×10^{-1}	0.7462	8.2×10^{-1}	0.7462	0.25×10	0.6368	93	3
Cu@Alg-FeNi5	4.6×10^{-1}	0.8443	9.8×10^{-1}	0.6872	9.8×10^{-1}	0.6872	0.48×10	0.6132	96	3

for Cu NPs is very efficient, as it completes the reaction in only 3–5 min. As demonstrated in the inset of Fig. 4e, the % reduction of 4NP is approximately 93% in Cu NPs supported on Alg-FeNi1, Alg-FeNi3, and Alg-FeNi5 in 5, 4, and 3 min respectively. Another important point mentioned in the literature is the induction period t_0. The induction period is considered an inactive period in the field of catalysis in which the catalyst activates its active sites for the reaction. The t_0 (2 min) is only observed in the Cu@Alg-FeNi1 catalyst, where one can see that the rate of reaction is swiftly enhanced after the induction period. The t_0 is reported from seconds to minutes in the literature [30].

Interestingly, after adding more FeNi in weight% to the alginate biopolymer, the induction period was not observed, and the catalyst activity was swift. As mentioned in Table 1, the rate of reactions (k_{aap}) and R^2 values were derived from various kinetics models. Among all the kinetics models, the experimental rate data is fitted in zero-order kinetics because of the high linearity of data. Similarly, the highest k_{app} value was displayed by Cu@Alg-FeNi5 3.8×10^{-1} min^{-1}, followed by Cu@Alg-FeNi3 and Cu@Alg-FeNi1. The data revealed that by increasing the inorganic filler FeNi to the alginate biopolymer, the active sites of Cu NPs are enhanced, and thus the reaction rate is enhanced. Other kinetics equations were employed, including pseudo-1st, 1st, and 2nd order kinetics, but as clear from Table 1; the data only fit in the zero-order kinetics models, which suggested that the rate of reaction does not depend on the concentration of reactants.

Discoloration of MB dye

Many attempts have been made to decolorize the MB dyes; however, zero-valent metal NPs application is one of the most important methods for this purpose. The cationic form of MB dye is its oxidized form with a maximum wavelength of 664 nm; however, after the addition of $NaBH_4$ MB, it converted to its oxidized form called the leuco MB dye. The leuco form of MB dye is colorless, appeared at λmax of the week, and had strong absorbance at 314 and 254 nm, respectively. The MB dye is decolorized and degraded slowly at λ_{max} 664 nm; however, after adding Cu NPs supported by different matrices, the reaction rate was swiftly enhanced. As mentioned in Fig. 5a, minor changes occurred after 9 min with $NaBH_4$, after the addition of the catalyst Cu@Alg-FeNi1-5 catalyst (Fig. 5b–d) respectively, the absorbance at λ_{max} 664 nm in 5, 3, and 3 min respectively. As evident from Table 2, the R^2 values are closer to 1 in zero-order kinetics compared to the other kinetics models. Therefore, it is inferred that the discoloration of MB dye in the presence of $NaBH_4$ with Cu NPs independent of the concentration of the MB dye or $NaBH_4$. Other researchers also used zero-order kinetics to reduce MB dye in the presence of $NaBH_4$ [31, 32]. Approximately 96% of MB dye was decolorized with Cu@Alg-FeNi5 NPs in only 3 min which supported the fact that FeNi NPs have a promising role in establishing the active site of Cu NPs in Cu@Alg-FeNi5 catalyst.

Concurrent Removal of a Mixture of 4NP and MB dye

For practical applicability, both 4NP and MB dye was mixed in a glass vial and then added $NaBH_4$ to the same vial. The $NaBH_4$ reacts with 4NP and MB to make its nitrophenolate ions and reduced form of MB dye. It is worth mentioning that the λ_{max} of 4-nitrophenolate ions is increased from 400 to 415 nm and MB dye from 664 to 675 nm. This indicates that approximately 15 and 11 nm increase was observed in the λ_{max} of 4-nitrophenolate anions and reduced form of MB dye. This is explained by the fact that there might be some weak force of interactions between the nitrophenolate and MB dye which brought a red shift in the mixture of 4NP and MB dye. The UV-Vis spectrum of 4NP + MB dye in the presence of $NaBH_4$ is presented in Fig. 6a. As seen in the range, both nitrophenolate and leuco MB dye species are present, suggesting that no chemical interactions have occurred after mixing the 4NP + MB + $NaBH_4$. Therefore, no extra peaks in the UV-Vis. spectrum was observed. Furthermore, the reaction proceedings for the 4NP + MB dye mixture were monitored for 9 min in the presence of $NaBH_4$ where no noticeable change in the absorbance was observed. The removal of 4NP + MB dye in $NaBH_4$ was further assessed

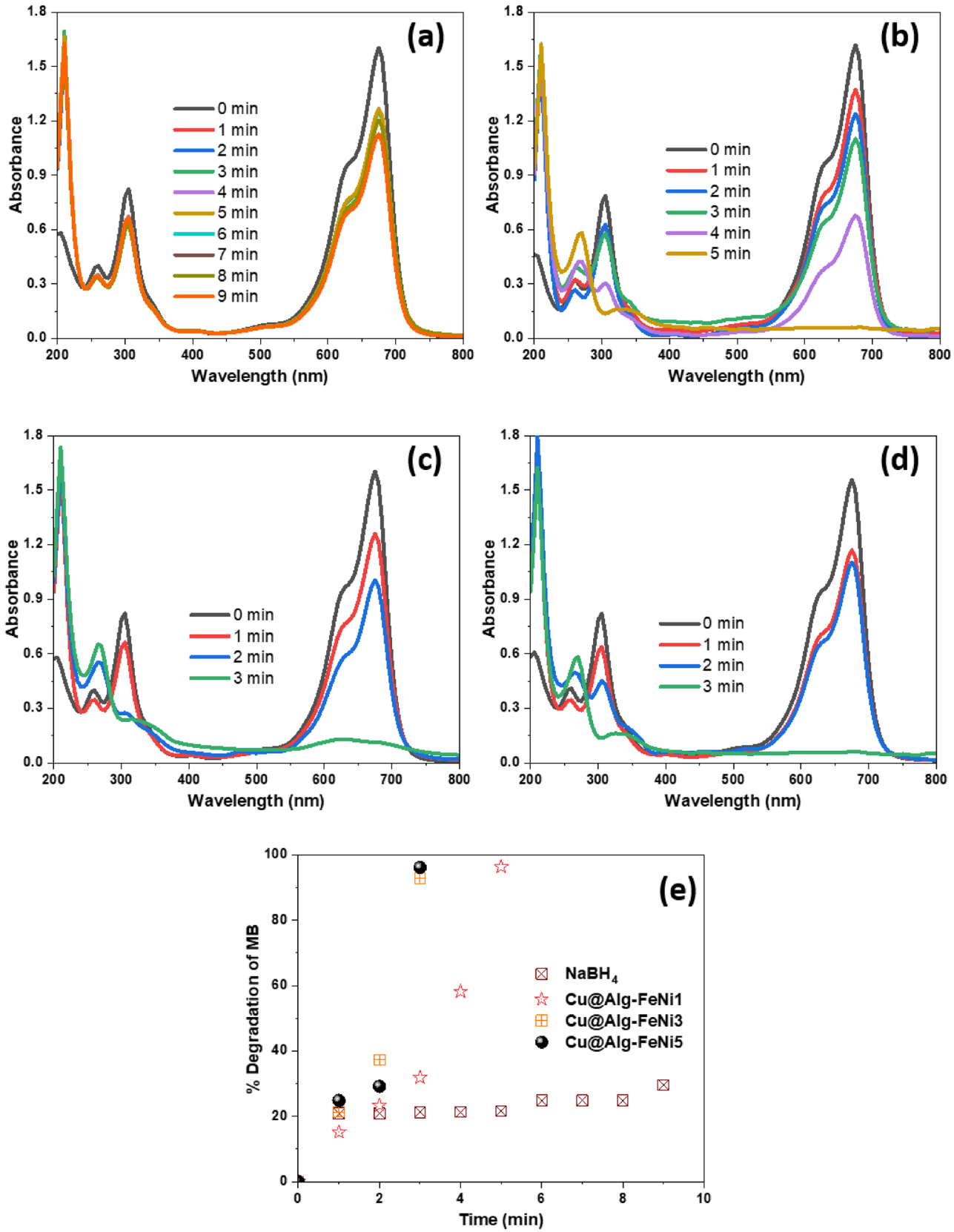

Fig. 5 UV-Visible spectrum of MB dye with $NaBH_4$ (**a**), Cu@Alg-FeNi1 (**b**), Cu@Alg-FeNi3 (**c**), Cu@Alg-FeNi5 (**d**), % discoloration of MB dye (**e**)

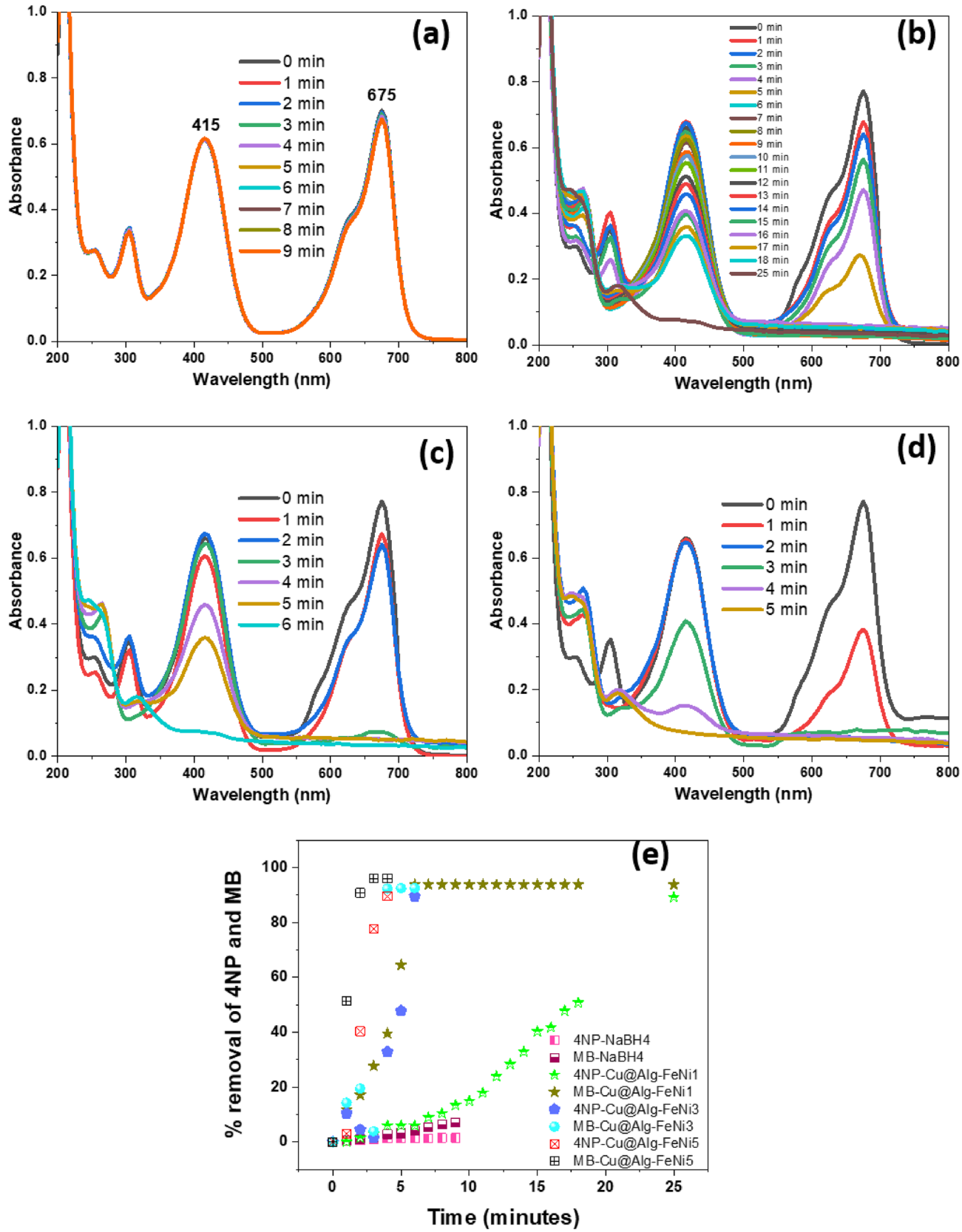

Fig. 6 Concurrent removal of 4NP and MB dyes with $NaBH_4$ (**a**), Cu@Alg-FeNi1 (**b**), Cu@Alg-FeNi3 (**c**), Cu@Alg-FeNi5 (**d**), and % removal of 4NP and MB as a function of time (**e**)

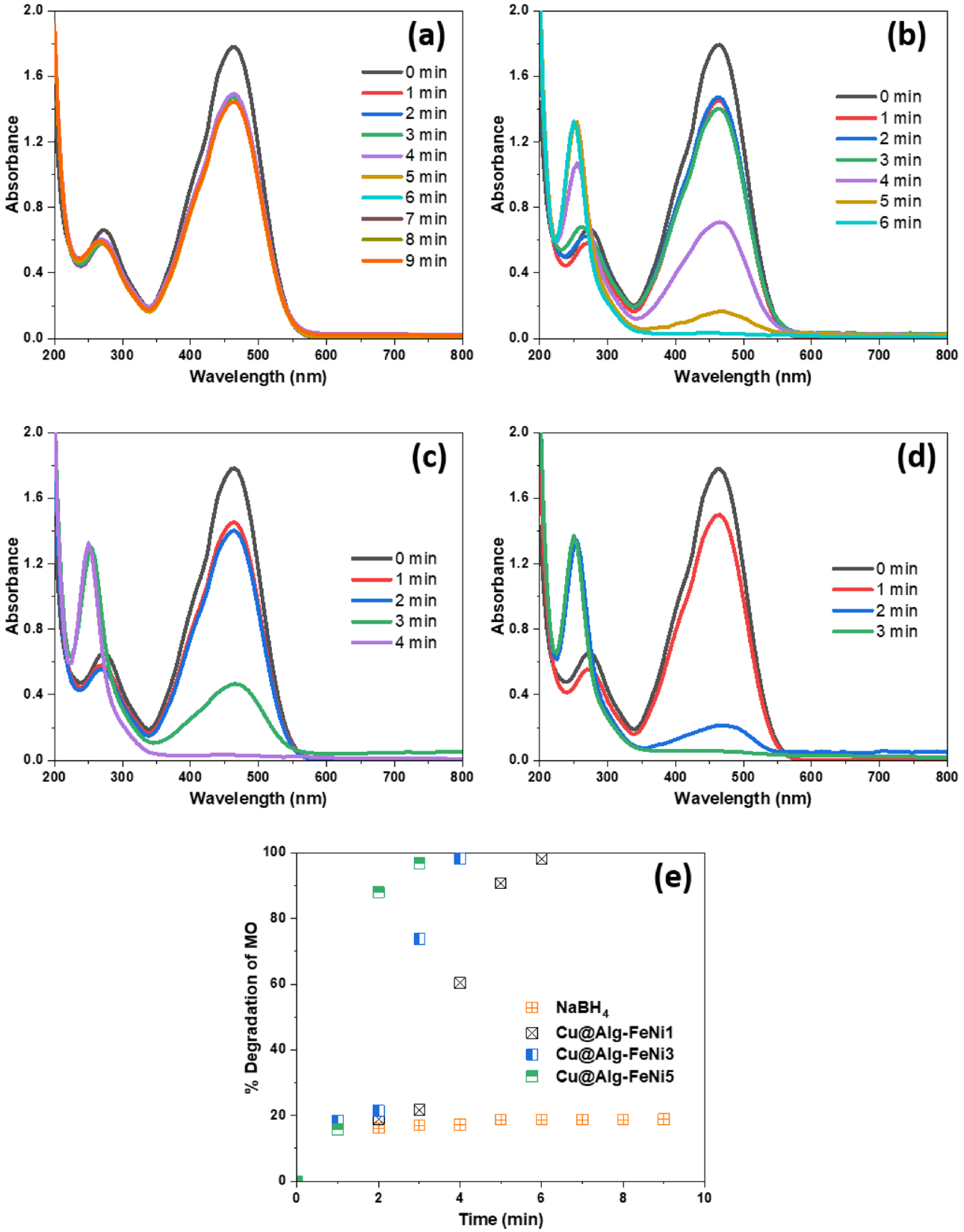

Fig. 7 UV-Visible spectrum of MO dye with $NaBH_4$ (**a**), Cu@Alg-FeNi1 (**b**), Cu@Alg-FeNi3 (**c**), Cu@Alg-FeNi5 (**d**), % degradation of MO dye (**e**)

Table 3 Rate constant and R^2 values of MO dyes derived from various kinetics models

Entry	Zero-order		Psuedo-1st		1st order		2nd order		Degradation	Time
	k_{app}	R^2	k_{app}	R^2	k_{app}	R^2	k_{app}	R^2	%	min^{-1}
$NaBH_4$	2.2×10^{-3}	0.4366	1.4×10^{-3}	0.4531	1.4×10^{-3}	0.4531	9.0×10^{-3}	0.4705	18	9
Cu@Alg-FeNi1	3.1×10^{-2}	0.9075	6.1×10^{-1}	0.7645	6.1×10^{-1}	0.7645	0.4×10	0.4964	98	6
Cu@Alg-FeNi3	4.5×10^{-1}	0.9168	9.1×10^{-1}	0.7451	9.1×10^{-1}	0.7451	0.6×10	0.5398	98	4
Cu@Alg-FeNi5	6.5×10^{-1}	0.9002	0.12×10	0.9239	0.1×10	0.9239	0.6×10	0.7794	96	3

in the presence of Cu@Alg-FeNi1 catalyst, and the reaction was observed for 25 min, where approximately both 4NP and MB dye derivatives were removed. It is worth mentioning that initially, the rate of MB dye discoloration was very fast, while the 4NP remained unaffected. However, after the removal of MB dye in approximately 6 min, the reduction of 4NP started and became faster when the MB dye was removed entirely (Fig. 6b). This data suggested that the catalyst is selective for MB dye compared to 4NP.

Similarly, the mixture mentioned above was remediated in Cu@Alg-FeNi3 and Cu@Alg-FeNi5 catalysts. The same discussion is valid for these catalyzed reactions as discussed for Cu@Alg-FeNi1. However, the rate of reactions was very fast with Cu@Alg-FeNi3 and Cu@Alg-FeNi5 catalysts. Like Cu@Alg-FeNi1, the Cu@Alg-FeNi3, and Cu@Alg-FeNi5 decolorized MB dye faster than 4NP (Fig. 6c and d). The 4NP reduction started after the discoloration of MB dye with all these catalysts. Figure 6e indicates the percentage degradation of concurrent removal of 4NP and MB dyes, in which MB dye degraded first, followed by 4NP reduction in the presence of $NaBH_4$.

Discoloration of MO dye

Figure 7a shows the degradation of MO dye was recorded for 9 min with $NaBH_4$ only, and one can see a little change in the absorbance of MO dye at 464 nm. However, after adding Cu@Alg-FeNi1-5 catalyst to MO dye solution in the presence of $NaBH_4$, the discoloration of MO dye was enhanced, and the orange color of MO dye vanished in 6, 4, and 3 min respectively (Fig. 7b–d). During the degradation of MO dye, a peak at 248 nm appeared in the absorbance spectrum, revealing the $–NH_2$–containing products. As mentioned in Table 3; Fig. 7e, approximately 98% of MO dye was degraded in 6 and 4 min with Cu@Alg-FeNi1 and Cu@Alg-FeNi3 catalysts, respectively, while 96% of MO dye was degraded in 3 min with Cu@Alg-FeNi5 catalyst. Different kinetics models were applied to deduce the rate constant values and linearity of the reactions, however, among all these models, zero-order kinetics was the most suitable because of the high linearity of data in this equation. By comparing the R2 values of all the kinetics models, the zero-order is described as the best model, and the experimental data agree with this model. Therefore, the reaction follows a zero-order kinetics model where the reaction rate is independent of the reactant concentration.

Recyclability Test

The recyclability of the catalyst is an essential parameter in the field of catalysis to assess the longer life of the catalyst. In the current work, 4NP was used as a pollutant, and Cu@Alg-FeNi5 catalyst was selected as a catalyst owing to its high catalyst potential against all 4NP reduction and MB and MO dye discoloration. The recyclability of the catalyst was checked for five cycles, as indicated in Fig. 8a–e, respectively. The first two cycles were completed in 5 min with approximately 92% reduction, while the third and fourth cycles were completed in 7 and 9 min, respectively, while the fifth cycle took a little longer and was completed in 13 min with a 92% reduction of 4NP. The decline in catalyst activity is due to the high transport of reactants on the active sites, and such trends are primarily encountered in catalysis [33]. Figure 8f indicates the % reduction of 4NP till the fifth cycle.

Conclusion

We have synthesized alginate biopolymer-FeNi blend beads templated zero-valent Cu NPs. The pure alginate beads were cross-linked with $CaCl_2$ solution. However, these beads are very labile and quickly dissolved in water for further chemical studies. Therefore, FeNi composite was added to the alginate biopolymer at different weight% such as 1, 3, and 5%. The synthesized Alg–FeNi1-5 catalysts were firm, not dissolved in water or solution, and were used for further chemical studies. The Cu@Alg-FeNi catalysts were characterized through FESEM, EDS, Raman, and XRD. The FESEM images indicated that Cu NPs are present in the internal of Alg-FeNi networking showing the stable nature of the catalyst. The stability

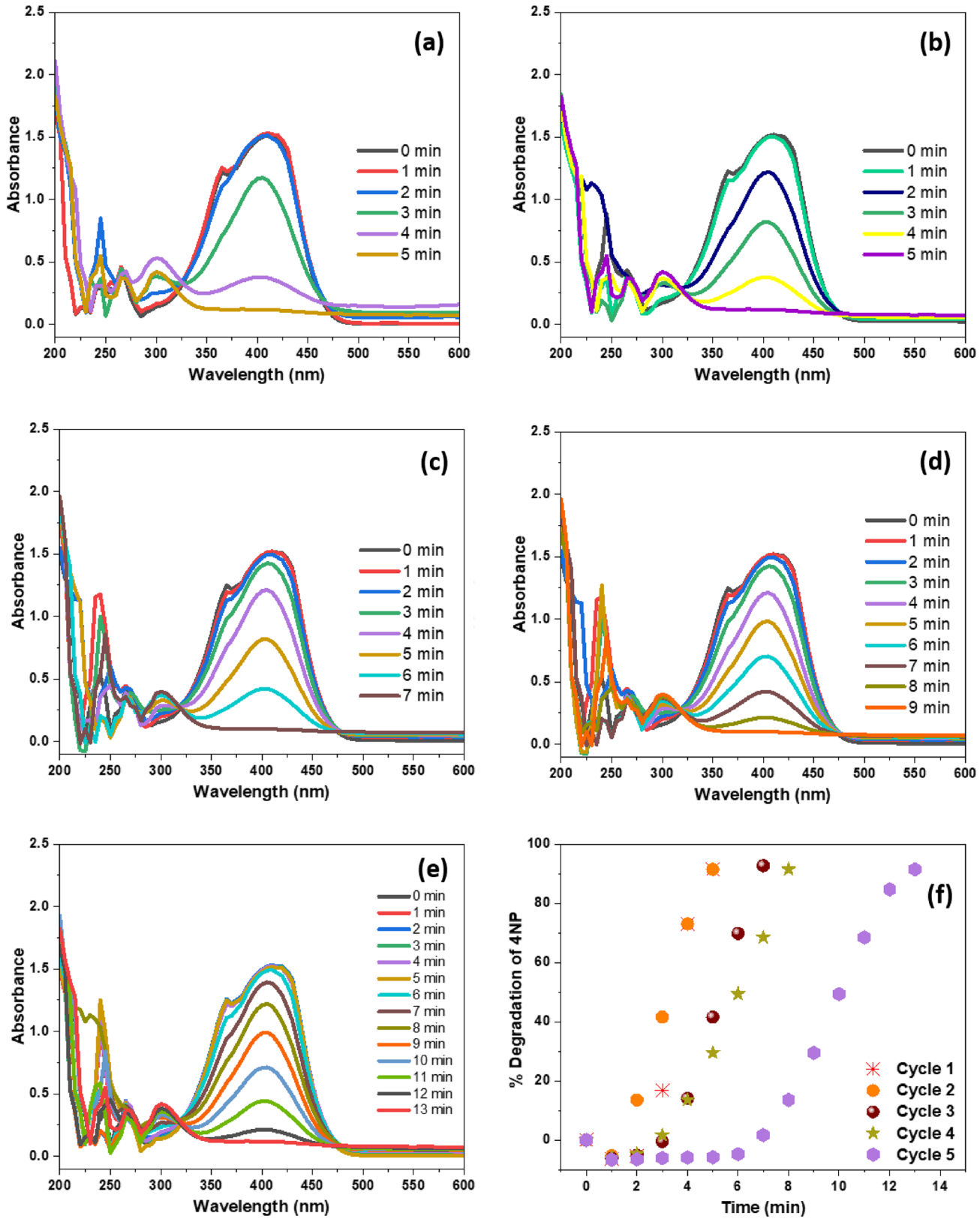

Fig. 8 UV-Vis. spectrum of 4NP reduction in the presence of $NaBH_4$ by using Cu@Alg-FeNi5 catalyst cycle 1 (**a**), cycle 2 (**b**), cycle 3 (**c**), cycle 4 (**d**), and cycle 5 (**e**), while percentage reduction of 4NP after a specific time (**f**)

was also revealed during the degradation of nitrophenol or dyes, where no leaching was observed visibly. Similarly, the EDS confirmed the purity of the catalyst and the amount of each element in the catalyst. At the same time, the Raman showed certain functional groups such as –COOH, C–H, O–H groups to confirm the structure of the catalyst, while the XRD clearly showed the crystalline peaks for Cu NPs, suggesting the presence of zero-valent Cu NPs. Catalysts were used against the sole and concurrent degradation of 4NP and MB dye, in which Cu@Alg-FeNi5 catalysts showed the most potent catalyst activity for sole and simultaneous degradation of 4NP and MB dye. This suggested that an increased amount of FeNi in the alginate biopolymer stabilized and activated the Cu NPs. The same catalyst also indicated vigorous activity against the discoloration of MO dye. Furthermore, the kinetics models revealed that all three pollutants (4NP, MB, and MO dyes) used in this experiment followed the zeroth order kinetics model. Thus, the reaction rate is independent of the concentration of reactants. The k_{app} values for 4NP reduction or MB, MO dye discoloration were the highest with Cu@Alg-FeNi5 catalyst. The three catalysts showed excellent activity in the degradation of nitrophenol or dyes and thus can be used in other potential applications.

Acknowledgements The author extends their appreciation to the deputyship for Research & Innovation, Ministry of Education in Saudi Arabia for funding this research work through the project number (IFP-2020-73).

Data Availability Data sharing does not apply to this paper.

Declarations

Conflict of interest The authors declare no conflict of interest.

References

1. Akhtar K, Khan SA, Khan SB, Asiri AM (2018) Nanomaterials and environmental remediation: a fundamental overview. Nanomater Environ Appl Fascin Attrib 2:1–36
2. Khan SA, Bakhsh EM, Asiri AM, Khan SB (2021) Chitosan coated NiAl layered double hydroxide microsphere templated zero-valent metal NPs for environmental remediation. J Clean Prod 285:124830
3. Varaprasad K, Jayaramudu T, Kanikireddy V, Toro C, Sadiku ER (2020) Alginate-based composite materials for wound dressing application: a mini review. Carbohydr Polym 236:116025
4. Šimkovic I (2008) What could be greener than composites made from polysaccharides? Carbohydr Polym 74:759–762
5. Khan SA, Bakhsh EM, Akhtar K, Khan SB (2020) A template of cellulose acetate polymer-ZnAl/C layered double hydroxide composite fabricated with Ni NPs: applications in the hydrogenation of nitrophenols and dyes degradation. Spectrochim Acta Part A Mol Biomol Spectrosc 241:118671
6. Ali I, Burakova I, Galunin E, Burakov A, Mkrtchyan E, Melezhik A, Kurnosov D, Tkachev A, Grachev V (2019) High-speed and high-capacity removal of methyl orange and malachite green in water using newly developed mesoporous carbon: kinetic and isotherm studies. ACS omega 4:19293–19306
7. Astrup T, Stipp S, Christensen TH (2000) Immobilization of chromate from coal fly ash leachate using an attenuating barrier containing zero-valent iron. Environ Sci Technol 34:4163–4168
8. Bakhsh EM, Khan SA, Marwani HM, Danish EY, Asiri AM, Khan SB (2018) Performance of cellulose acetate-ferric oxide nanocomposite supported metal catalysts toward the reduction of environmental pollutants. Int J Biol Macromol 107:668–677
9. Ismail M, Khan M, Khan SA, Qayum M, Khan MA, Anwar Y, Akhtar K, Asiri AM, Khan SB (2018) Green synthesis of antibacterial bimetallic Ag–Cu nanoparticles for catalytic reduction of persistent organic pollutants. J Mater Sci: Mater Electron 29:20840–20855
10. Khan SA, Bello BA, Khan JA, Anwar Y, Mirza MB, Qadri F, Farooq A, Adam IK, Asiri AM, Khan SB (2018) Albizia chevalier based Ag nanoparticles: anti-proliferation, bactericidal and pollutants degradation performance. J Photochem Photobiol B 182:62–70
11. Khan SA, Ismail M, Anwar Y, Farooq A, Al Johny BO, Akhtar K, Shah ZA, Nadeem M, Raza MA, Asiri AM (2019a) A highly efficient and multifunctional biomass are supporting Ag, Ni, and Cu nanoparticles through wetness impregnation for environmental remediation. Green Process Synthesis 8:309–319
12. Nodeh HR, Ibrahim WAW, Ali I, Sanagi MM (2016) Development of magnetic graphene oxide adsorbent for the removal and preconcentration of As (III) and As (V) species from environmental water samples. Environ Sci Pollut Res 23:9759–9773
13. Saravanan R, Thirumal E, Gupta V, Narayanan V, Stephen A (2013) The photocatalytic activity of ZnO prepared by simple thermal decomposition method at various temperatures. J Mol Liq 177:394–401
14. Saravanan R, Gupta V, Narayanan V, Stephen A (2014) Visible light degradation of textile effluent using novel catalyst ZnO/γ-Mn2O3. J Taiwan Inst Chem Eng 45:1910–1917
15. Shaari N, Kamarudin S (2015) Chitosan and alginate types of bio-membrane in fuel cell application: an overview. J Power Sources 289:71–80
16. Shchukin DG, Radtchenko IL, Sukhorukov GB (2003) Synthesis of nanosized magnetic ferrite particles inside hollow polyelectrolyte capsules. J Phys Chem B 107:86–90
17. Ali HSHM, Khan SA (2020) Stabilization of various zero-valent metal nanoparticles on a superabsorbent polymer for the removal of dyes, nitrophenol, and pathogenic bacteria. ACS Omega 5:7379–7391
18. Ali I, Alharbi OM, Alothman ZA, Alwarthan A (2018) Facile and eco-friendly synthesis of functionalized iron nanoparticles for cyanazine removal in water. Colloids Surf B 171:606–613
19. Gupta VK, Atar N, Yola ML, Üstündağ Z, Uzun L (2014) A novel magnetic Fe@ Au core–shell nanoparticles anchored graphene oxide recyclable nanocatalyst for the reduction of nitrophenol compounds. Water Res 48:210–217
20. Khan SA, Khan N, Irum U, Farooq A, Asiri AM, Bakhsh EM, Khan SB (2020) Cellulose acetate-Ce/Zr@ Cu0 catalyst for the degradation of organic pollutant. Int J Biol Macromol 153:806–816
21. Khan SA, Khan SB, Farooq A, Asiri AM (2019b) A facile synthesis of CuAg nanoparticles on highly porous ZnO/carbon black-cellulose acetate sheets for nitroarene and azo dyes reduction/degradation. Int J Biol Macromol 130:288–299
22. Pradhan N, Pal A, Pal T (2002) Silver nanoparticle catalyzed reduction of aromatic nitro compounds. Colloids Surf A 196:247–257

23. Sohni S, Khan SA, Akhtar K, Khan SB, Asiri AM, Hashim R, Omar AM (2018) Room temperature preparation of lignocellulosic biomass supported heterostructure (Cu + Co@ OPF) as highly efficient multifunctional nanocatalyst using wetness co-impregnation. Colloids Surf A 549:184–195
24. Khan SA, Khan SB, Asiri AM (2016a) Layered double hydroxide of Cd-Al/C for the mineralization and de-coloration of dyes in solar and visible light exposure. Sci Rep 6:1–15
25. Khan SA, Khan SB, Asiri AM (2016b) Toward the design of Zn–Al and Zn–Cr LDH wrapped in activated carbon for the solar assisted de-coloration of organic dyes. RSC Adv 6:83196–83208
26. Manzoor J, Sharma M (2020) Impact of textile dyes on human health and environment. In: Impact of textile dyes on public health and the environment. IGI Global, pp 162–169. https://doi.org/10.4018/978-1-7998-0311-9.ch008
27. Kaleem U, Salman K, Musa K, Zia UR, Youssef OA, Azhar M, Shah H, Sher BK, Shahid AK (2022) A bioresource catalyst system of alginate-starch-activated carbon microsphere templated Cu nanoparticles: Potentials in nitroarenes hydrogenation and dyes discoloration. Int J Biol Macromol 222:887–901
28. Oliani WL, Parra DF, Komatsu LGH, Lincopan N, Rangari VK, Lugao AB (2017) Fabrication of polypropylene/silver nanocomposites for biocidal applications. Mater Sci Engineering: C 75:845–853
29. Miranda AM, Castilho-Almeida EW, Ferreira EHM, Moreira GF, Achete CA, Armond RA, Dos Santos HF, Jorio A (2014) Line shape analysis of the Raman spectra from pure and mixed biofuels esters compounds. Fuel 115:118–125
30. Siyam MA, Christopher LK (2016) Impact of gold nanoparticle stabilizing ligands on the colloidal catalytic reduction of 4-nitrophenol. ACS Catal 6:5553–5560
31. Misbah S, Asma J, Maliha U, Muhammad I, Farhat J, Shazia N, Nazish S, Ismat B, Rashid M, Waqas A (2018) Linear and crosslinked Polyurethanes based catalysts for reduction of methylene blue. J Hazard Mater 344:210–219
32. Vasanthakumar A, Pavithra S, Ta-Jen Y, Gyanasivan GR, Robert MG (2018) Nano-material as an excellent catalyst for reducing a series of nitroanilines and dyes: triphosphonated ionic liquid-CuFe2O4-modified boron nitride. Appl Catal B 222:99–114
33. Sher BK, Mohammad SJK, Tahseen K, Abdullah MA, Esraa MB (2020) Polymer supported metallic nanoparticles as a solid catalyst for the removal of organic pollutants. Cellulose 27:5907–5921

Publisher's Note Springer Nature remains neutral with regard to jurisdictional claims in published maps and institutional affiliations.

Springer Nature or its licensor (e.g. a society or other partner) holds exclusive rights to this article under a publishing agreement with the author(s) or other rightsholder(s); author self-archiving of the accepted manuscript version of this article is solely governed by the terms of such publishing agreement and applicable law.